Synthetic Polymers and Biomembranes. How Do They Interact?: Atomistic Molecular Dynamics Simulation Study of PEO in Contact with a DMPC Lipid Bilayer

Sandeep Pal,[†] Giuseppe Milano,*[,‡] and Danilo Roccatano*[,§]

Biosystems Informatics Institute, Bioscience Centre, International Centre for Life Times Square, NE1 4EP Newcastle upon Tyne, United Kingdom, Department of Chemistry, University of Salerno, Via Salvador Allende, I-84081 Baronissi, Salerno, Italy, and School of Engineering and Science, International University of Bremen,[||] Campus Ring 1, D-28725 Bremen, Germany

Received: June 2, 2006; In Final Form: September 23, 2006

The understanding of interactions of poly(ethylene glycol) (PEG) or poly(ethylene oxide) (PEO) with biological interfaces has important technological application in industry and in medicine. In this paper, structural and dynamical properties of PEO at the dimyristoylphospatidylcholine (DMPC) bilayer/water interface have been investigated by molecular dynamics (MD) and steered molecular dynamics (SMD) simulations. The structural properties of a PEO chain in bulk water, at the water/vacuum interface, and in the presence of the membrane were compared with available experimental data. The presence of a barrier for the PEO penetration into the DMPC bilayer has been found. A qualitative estimation of the barrier provided a value equal to ∼19 kJ/mol, that is, 7 times the value of *kT* at 310 K.

1. Introduction

The use of synthetic polymers for biomedical applications has rapidly grown in past years.[1] Synthetic polymers are particularly well-suited for implementing physical, chemical, and biological functions at the same time, and they permit the length scales to be greatly varied, the superstructure to be controlled, and specific functions to be performed. There is a wide variety of functional polymers capable of adopting functions such as encapsulation, stealth, cell adhesion, and cell recognition, as well as different actuator functions. These features are influenced predominantly by the polymer surface. Polymers with hydrophilic surfaces are often well-suited and so are those with an inert surface. Hydrophilic, noninteracting materials cannot be recognized by living systems (stealth systems) and therefore have low cytotoxicity. It is often advantageous to introduce functional groups into the polymer chain in order to bind bioactive molecules such as peptides, oligosaccharides, and antibodies. Among the polymers that have a broad use in this sector, poly(ethylene oxide) (PEO) or poly(ethylene glycol) (PEG) as homopolymer (see Scheme 1), grafted or as block copolymer, are the most popular.[2]

In fact, PEO is highly hydrophilic and shows a very low toxicity with respect to similar polymers. Currently research is increasingly being done in the field of drug delivery and drug targeting on a molecular level. Also, in this case, synthetic macromolecules offer a wide variety of possibilities as specific transportation systems in biology and medicine. They allow a large number of functions in a molecule to be combined. Small molecules cannot cope with such a number of functions.[3] One problem when using high molecular weight active ingredients is proteolytic decomposition that can be suppressed by encapsulation in polymers. Furthermore, their biodistribution can be regulated by surface modification, by introducing PEO (stealth systems) or monoclonal antibodies (site-specific targeting). By these means, the residence time, bioavailability, and permeability of polymeric active agents can be increased. After the polymers have been transported to the place of their target, the active agent is released. This takes place either by depolymerization or by splitting the active component from the polymer, by a swelling of the polymer and resulting release of the active ingredient, or by effusion of the active agent. Amphiphilic polymers and their association structures are of increasing interest as carriers of active ingredients.[4] Block copolymer micelles are being investigated in many research groups as carriers of hydrophobic active agents and genes. Their core/shell structure resembles that of lipoproteins and viruses.[5] The micelle shell causes the interaction with proteins and cells. These interactions decide on the biodistribution of the active component. The high activity of PEO/agent conjugates is believed to be closely connected with a special transport behavior through biological barriers. PEO influences the microviscosity and permeability of cell membranes.[6] This is the result of a special property of PEO: at a high degree of hydration in aqueous media PEO is hydrophilic, while at a low degree of hydration in hydrophobic environment it is, however, hydrophobic. Thus, PEO can be dehydrated at hydrophobic surfaces and can be transported into or through these boundary surfaces. Interest in polymeric materials based on PEO stems primarily from potential application as inexpensive, readily available substitutes for more expensive lipid-grafted polymers (lipopolymers) in the preparation of sterically stabilized liposomes for drug delivery.[7] Another area of potential promise is their use in the sealing of damaged or permeabilized cell membranes following trauma.[8]

SCHEME 1: Repeating Unit of a PEO/PEG Chain

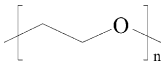

The penetration and accumulation of PEO in hydrophobic lipid layers was proven by X-ray diffraction studies. PEO-PPO-

* Corresponding author. E-mail: gmilano@unisa.it (G.M.); d.roccatano@iu-bremen.de (D.R.).
[†] International Centre for Life Times Square.
[‡] University of Salerno.
[§] International University of Bremen.
[||] Jacobs University Bremen as of spring 2007.

10.1021/jp063418d CCC: $33.50
Published on Web 12/21/2006

TABLE 1: Geometry and Force Field Parameters for PEO

Atomic Mass (u)		
CH_2	m	14.0270
O	m	15.9994
Bond Length Constraints (nm)		
CH_2-CH_2		0.144
CH_2-O		0.140
Angle Potential ϕ_0 (deg), k_ϕ [kJ/(mol rad^2)]		
CH_2-O-CH_2	ϕ_0	109.5
	k_ϕ	502.416
CH_2-CH_2-O	ϕ_0	109.5
	k_ϕ	418.680

Torsions Ryckaert−Bellemans functions [kJ/mol]

	C_0	C_1	C_2	C_3
CH_2-O-CH_2-O	1.71659	2.84702	1.04670	−5.61031
$O-CH_2-CH_2-O$	−1.15137	1.15137	0	0

Nonbonded Parameters

	C_6 [(kJ/mol) nm^6]	C_{12} [(kJ/mol) nm^{12}]	charges [q/ e]
CH_2	$5.947\,00 \times 10^{-3}$	$1.790\,000 \times 10^{-6}$	+0.15
O	$2.075\,08 \times 10^{-3}$	$1.512\,736 \times 10^{-6}$	−0.30

PEO triblock[9] and PEO-PPO diblock[10] copolymer interactions with lipid bilayers have been studied by Firestone and Seifert using small-angle X-ray scattering, wide-angle X-ray scattering, and differential scanning calorimetry. Recently Szleifer et al.[11] reported the effect of PEO on the DMPC bilayer at different concentrations of PEO. Their experimental and theoretical (single-chain mean field theory) studies were done to determine the phase diagram of the PEO/DMPC system at different concentrations and molecular weights of PEO. Their studies show that at low concentrations PEO is present at the outer monolayer of the bilayer.

Several atomistic and coarse-grained simulation studies on the lipid bilayers have been already performed by different groups.[12,13] Despite the spread in biomedical application of these materials, atomistic simulation studies of the interaction of PEO/PEG chain with biological membranes is still lacking.

In this paper, we report a detailed study of the properties of a 43 monomer long PEO chain at the interface with a DMPC bilayer with molecular dynamics (MD) and steered molecular dynamics (SMD) simulations.

The molecular dynamics simulations study was performed on three systems: PEO in bulk water (system 1), PEO at the water/vacuum interface (system 2), and PEO at the DMPC/water interface (system 3). The systems were studied using classical molecular dynamics (MD) simulations and, in the case of system 3, by steered molecular dynamics simulations also.[14]

2. Computational Details

Force Field. For the DMPC lipid bilayer, the united atom model by Berger et al.[15] was used. This model has been previously validated.[16,17] The model is essentially based on the GROMOS force field for lipid head groups, the Ryckaert−Bellemans potential[18] for hydrocarbon chains, and the OPLS parameters[19,20] for the Lennard-Jones (LJ) interactions between united CH_n groups of acyl chains reparametrized to reproduce experimentally observed values of volume per lipid.[21]

The aliphatic carbon atoms of the PEO were considered united atoms using, for the LJ parameters, the same adopted for the lipid atoms. Partial charges and bonded interaction parameters were adapted from the model reported by Kolafa and Ratner.[22] Table 1 contains a complete list of PEO parameters.

CHART 1: Schematic Setup Used To Perform the SMD Simulation

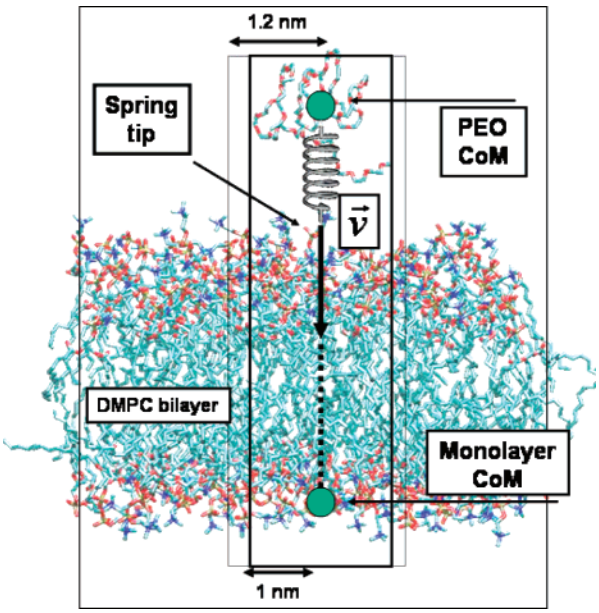

Simulation Details and Setups. *PEO in Bulk Water and at Water/Vacuum Interface.* A PEO chain of 43 monomers was used to study the properties of the polymer in water. The polymer was partially collapsed from an elongated chain, by a short MD simulation in vacuo. The obtained structure was solvated in a cubic box containing 3655 SPC model[23] water molecules.

Simulations were performed in the NPT ensemble (constant pressure and temperature ensemble) with the set values of the temperature and pressure being 310 K and 1 atm. The temperature and pressure were maintained around the set values using a Berendsen thermostat and barostat[24] with a coupling time constant of 0.1 ps for temperature and 0.5 ps for the pressure coupling.

The water/vacuum interface was prepared by expanding along the Z direction the equilibrated box of PEO water. The final dimension of the starting simulation box was $6.54 \times 6.54 \times 10.05$ nm^3. The system was simulated at constant volume and temperature (NVT) conditions for 20 ns.

PEO at Water/DMPC Interface. The periodic simulation box (having a size of $6.34 \times 6.36 \times 9.36$ nm^3), for the MD of the PEO/water/DMPC system, consists of a lipid bilayer of $N = 128$ DMPC molecules (64 molecules in each monolayer). The starting position of the PEO molecule was placed in the water layer at more than 4.5 nm away from the membrane interface. The nonbonded electrostatic interactions were calculated using the particle mesh Ewalds (PME)[25] method. For the calculation, a grid spacing of 0.12 nm combined with a fourth-order B-spline interpolation was used to compute the potential and forces between grid points. The Lennard-Jones interactions were calculated using a pair-list with a cutoff of 1.0 nm and updated every 10 time steps. A dielectric permittivity $\epsilon_r = 1$ was used.

The simulations of the PEO/DMPC/water system were performed in the NPT ensemble (constant pressure and temperature ensemble) with the set value of the temperature and pressure being 310 K and 1 atm, well above the DMPC gel/liquid crystalline transition temperature. The temperature and pressure were maintained around the set value using a Berendsen thermostat and barostat[24] with a coupling time constant of 0.1 ps for temperature and 0.5 ps for the pressure coupling. The

TABLE 2: Calculated PEO End-to-end Distances

system	$\langle L^2\rangle^{1/2}$ (nm)	$\langle L_X^2\rangle^{1/2}$ (nm)	$\langle L_Y^2\rangle^{1/2}$ (nm)	$\langle L_Z^2\rangle^{1/2}$ (nm)	$\langle L_Z^2\rangle^{1/2}/\langle L_{XY}^2\rangle^{1/2}$ [a]
PEO/bulk/water	1.28 ± 0.43	0.62 ± 0.42	0.65 ± 0.46	0.63 ± 0.46	0.97
PEO/water/vacuum	1.45 ± 0.50	0.89 ± 0.55	0.84 ± 0.57	0.37 ± 0.29	0.43
PEO/water/DMPC	1.23 ± 0.52	0.56 ± 0.40	0.54 ± 0.42	0.73 ± 0.57	1.30
PEO/water/DMPC [4−10 ns]	1.50 ± 0.60	0.52 ± 0.37	0.50 ± 0.41	1.15 ± 0.67	2.24

[a] $L_{XY} = 0.5(L_X + L_Y)$.

TABLE 3: Calculated PEO Radii of Gyration

system	$\langle R_g^2\rangle^{1/2}$ (nm)	$\langle R_{gX}^2\rangle^{1/2}$ (nm)	$\langle R_{gY}^2\rangle^{1/2}$ (nm)	$\langle R_{gZ}^2\rangle^{1/2}$ (nm)	$\langle R_{gZ}^2\rangle^{1/2}/\langle R_{gXY}^2\rangle^{1/2}$ [a]
PEO/bulk water	0.71 ± 0.04	0.41 ± 0.06	0.41 ± 0.07	0.40 ± 0.06	0.98
PEO/water/vacuum	0.72 ± 0.04	0.43 ± 0.08	0.40 ± 0.05	0.40 ± 0.04	0.96
PEO/water/DMPC	0.71 ± 0.04	0.40 ± 0.06	0.41 ± 0.06	0.42 ± 0.07	1.03
PEO/water/DMPC [4−10 ns]	0.72 ± 0.05	0.39 ± 0.06	0.41 ± 0.06	0.43 ± 0.08	1.10

[a] $R_{gxy} = 0.5(R_{gx} + R_{gy})$.

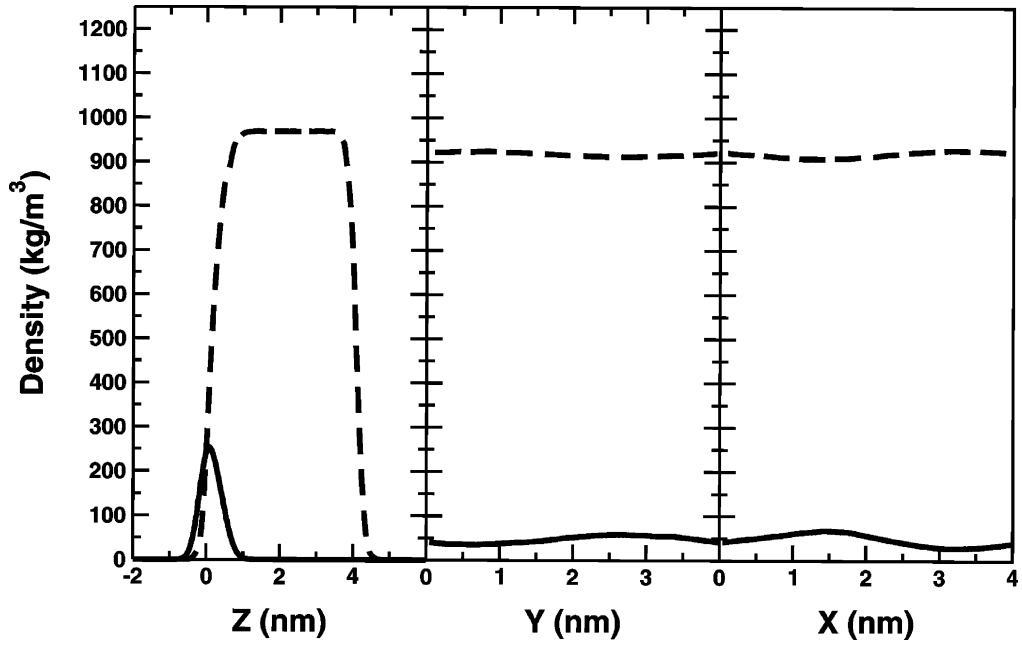

Figure 1. Density distribution inside the simulation box PEO/water vacuum interface (system 2).

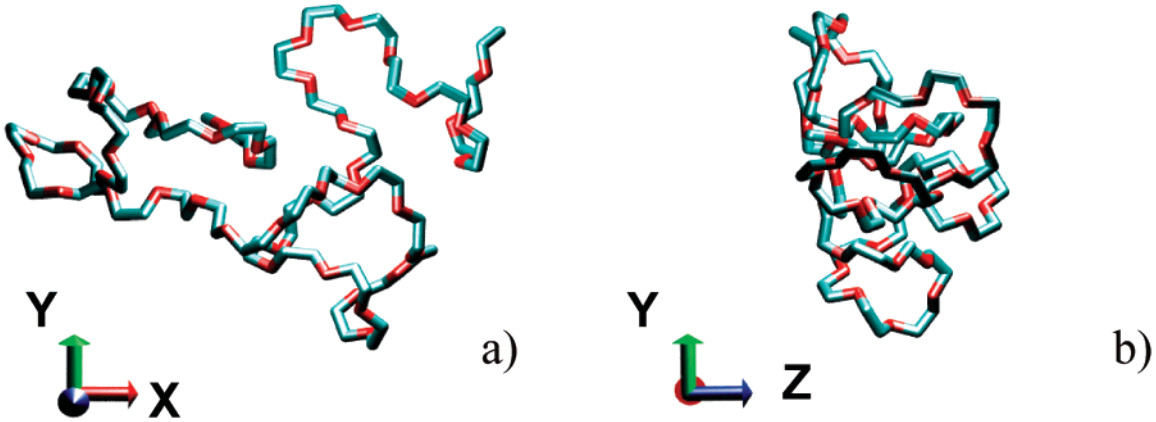

Figure 2. Snapshot of the PEO chain at the water/vacuum interface (system 2): (a) view perpendicular and (b) view parallel to the interface.

temperature coupling was applied separately for the lipid, PEO, and water. Pressure coupling was applied semiisotropically. The extension of the simulation box in the direction perpendicular to the bilayer surface (Z direction) and the cross-sectional area of the box in the $X-Y$ plane were allowed to vary independently of each other.[26] All bond lengths for the lipids and PEO molecule were constrained to their equilibrium values using the SHAKE algorithm,[27] whereas the SETTLE algorithm[28] was used for water molecules. The time step in all simulations was set to 2 fs.

Steered Molecular Dynamics Simulations. Steered molecular dynamics (SMD) method[14] was used to reduce the time scale required to have a spontaneous diffusion of PEO through one of the monolayers of the DMPC bilayer. The SMD

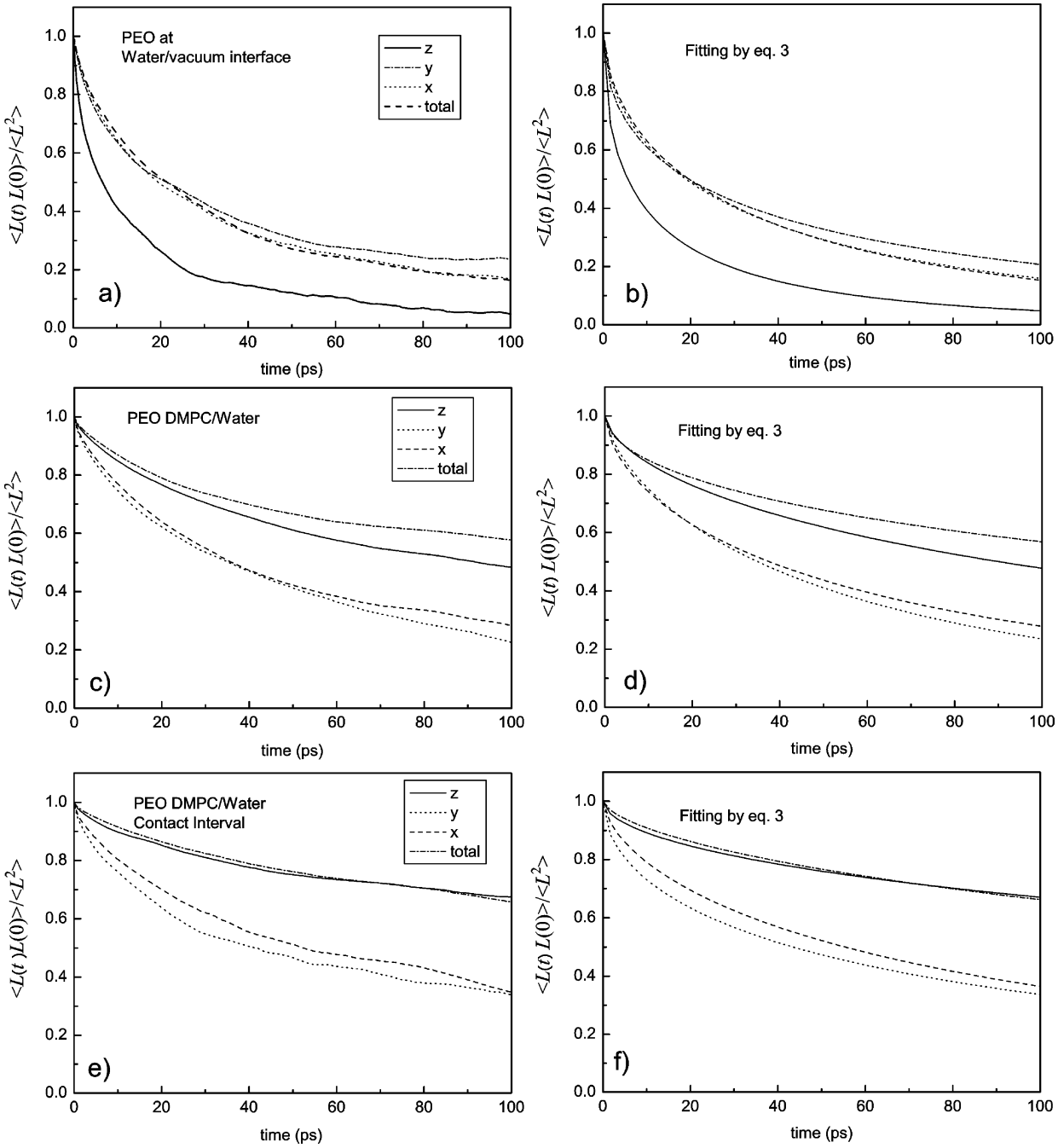

Figure 3. End-to-end time autocorrelation functions for the PEO chain (a) at the water/vacuum interface; (b) fitting of the curve of Figure 8a; (c) at DMPC/water interface; (d) fitting of curve of Figure 8c; (e) at the DMPC/water interface (contact time); (f) fitting of curve of Figure 8e.

TABLE 4: Calculated End-to-End Distance Relaxation Times

system	τ (ps)	τ_X (ps)	τ_Y (ps)	τ_Z (ps)
PEO/water/vacuum interface	57	58	55	20
PEO/water/DMPC	250	80	95	427
PEO/water/DMPC [4−10 $\nu\sigma$	302	148	139	397

simulation should be performed using a slow pulling regime to ensure operation in near-equilibrium conditions.[14]

Chart 1 shows the schematic setup used to perform the SMD simulation. The same methodology has been employed to study diffusion through the biological membrane of different solutes.[29−32] The center of mass (CoM) of PEO was harmonically restrained to a spring of force constant k. The spring tip is pulled with a constant velocity υ toward the CoM of the DMPC bottom monolayer (reference position). To compensate the lateral diffusion of the PEO that would affect the direction of the applied force, the reference position was calculated using the lipids, in the bottom monolayer, contained in a cylinder of radius 1.0 nm with axes parallel to the Z direction and passing trough the CoM of the PEO. The monolayer reference position was re-updated when the PEO CoM moved 0.2 nm away from the original position. During the pulling simulations, the force exerted on PEO, due to the extension of the moving spring, is given as $\mathbf{F} = k(z-\upsilon t)$, where z is the position of the CoM of the PEO and t is the time elapsed during the simulation. The value for $k = 200$ kJ mol^{-1} was chosen for all the simulations. Starting from a value of 5×10^{-4} nm/ps, the velocity was progressively decreased until no further variation in the DMPC penetration barrier height was observed. The pulling experiments with velocities of 1×10^{-4} and 5×10^{-5} nm/ps showed similar barrier heights, which were the eventual choices for the pulling

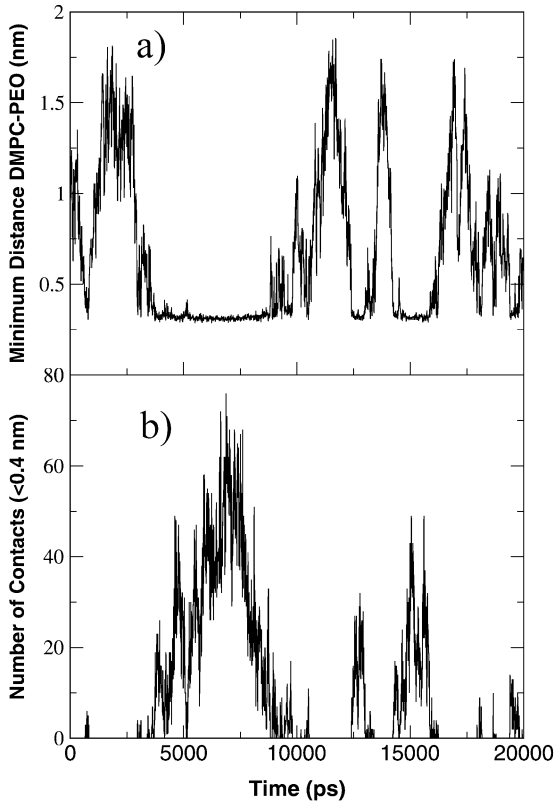

Figure 4. Time evolution of (a) the minimum distance and (b) number of contacts between PEO and DMPC bilayers.

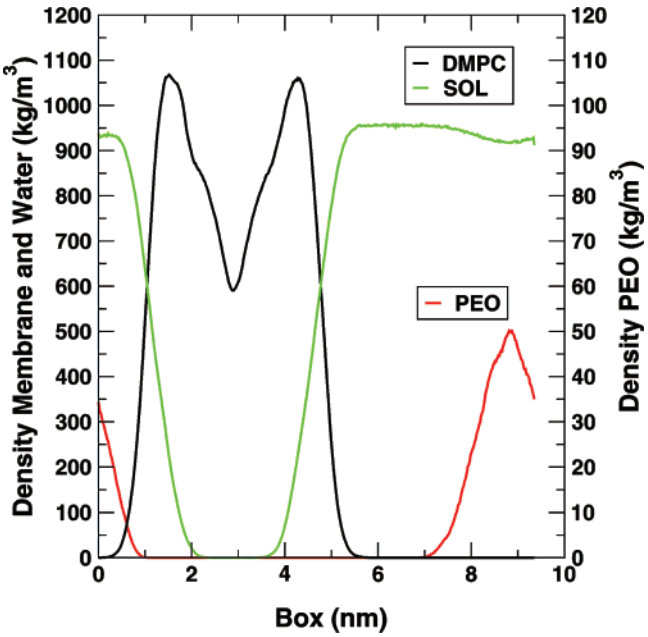

Figure 5. Averaged density distributions of the PEO (red), lipids (black), and water (green) along the *Z* axis of the simulation box for system 2. The average was performed along the last 5 ns of the simulation.

simulations. Five pulling simulations were performed. One simulation was performed using a pulling velocity $v = 5 \times 10^{-5}$ nm/s, whereas the other four, using the same pulling velocity $v = 1 \times 10^{-4}$ nm/s but different starting PEO position. All SMD simulations were run for a time of 10 ns.

All the simulations reported in the present paper were performed using GROMACS.[33,34] Pictures of structures obtained from simulations have been made by VMD program.[35]

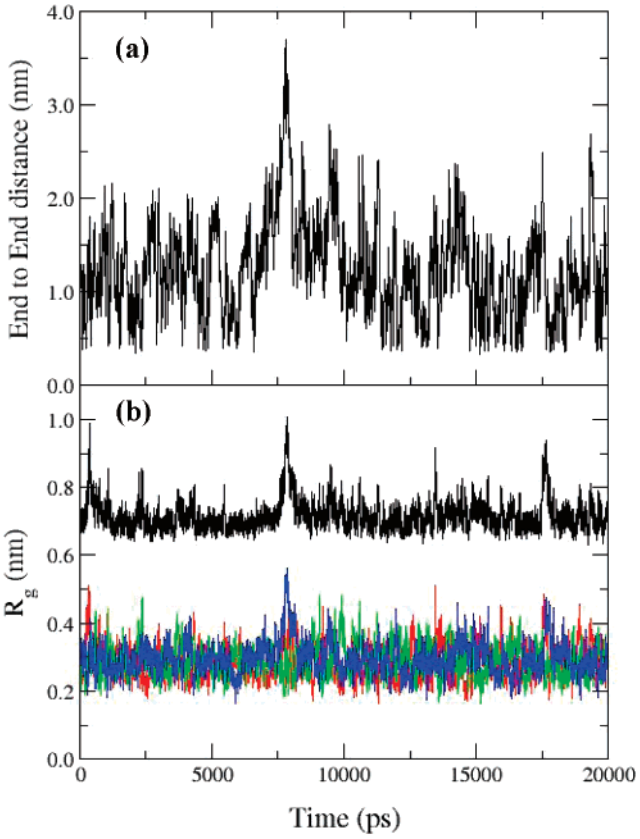

Figure 6. Time evolution of the PEO (a) end-to-end distance and (b) radius of gyration during the system 2 simulation.

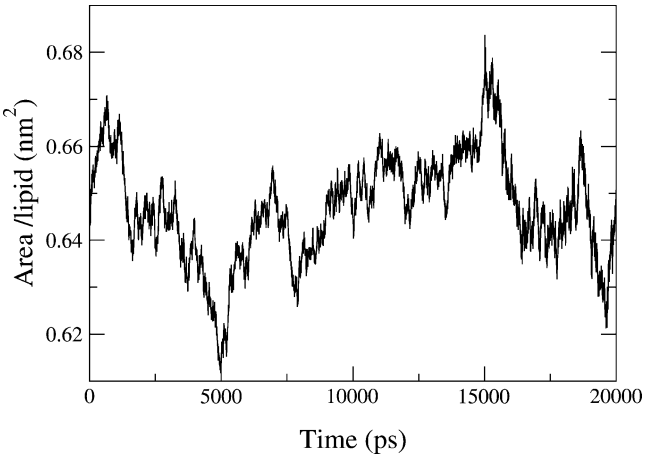

Figure 7. Time evolution of the area per lipid for system 2.

3. Results and Discussion

PEO in Bulk Water and at Water/Vacuum Interface. *Chain Structure and Dynamics.* In order to investigate the effect of a pure hydrophobic surface on the polymer structure and dynamics, the PEO chain has been simulated in the presence of a water/vacuum interface and for comparison in bulk water. In both cases, structural and dynamical properties were calculated and compared with the experimental values available.

In Tables 2 and 3, calculated end-to-end distances (L) and radii of gyration (R_g) for the different systems considered have been reported. When the polymer chain is in the presence of an interface, as in the case of systems 2 and 3, the $X-Z$ components of both L and R_g are also reported. In these cases, the Z direction has been assumed the one perpendicular to the interface.

The calculated average radius of gyration and end-to-end distance of a 43-mer PEO in bulk water are 0.71 ± 0.01 and 1.28 ± 0.43 nm, respectively. The experimental chain size in water was estimated by fitting the experimental values of R_g as a function of molecular weight in the range of 17 000−61 000 using an exponential law:[36]

$$\langle R_g \rangle = aN^{\nu} \quad (1)$$

From the fitting, the values of $a = 0.0869$ nm and $\nu = 0.59$ were obtained. The exponent value is in agreement with the Flory's theory[37] of polymer chains in good solvent. Using the fitted values, an $R_g \sim 0.8$ nm was derived for the 43-mer PEO chain.

In presence of the water/vacuum interface (system 2), the R_g value (0.72 nm) is almost unchanged with respect to that in bulk water, while the L value is slightly higher (1.45 nm). In particular, the X and Y components of L parallel to the interface are about 1.5 times larger than the values calculated in bulk water, while the Z component perpendicular to the interface is almost half of the bulk value.

In Figure 1, the density distribution inside the simulation box for system 2 is reported. It is worth a mention that the PEO distribution shows a peak close to the water/vacuum interface. In Figure 2, a snapshot of the PEO chain in system 2 after 5 ns is reported. The figure clearly shows the tendency of the polymer chain to elongate in the X and Y directions (parallel to the interface) with respect to the Z direction (perpendicular to the interface).

In order to characterize the global relaxation of the PEO chain in the three systems considered, the time autocorrelation functions $C(t)$ for the end-to-end vector **L** were calculated:

$$C(t) = \frac{\langle \mathbf{L}(0)\cdot\mathbf{L}(t)\rangle}{\langle \mathbf{L}^2\rangle} \quad (2)$$

To obtain a relaxation time, $C(t)$ was fitted to the stretched exponential (Kohlrausch−Williams−Watts)[38] functional form:

$$C(t) = \exp[-(t/\alpha)^{\beta}] \quad (3)$$

The relaxation time equals then the time integral of the stretched exponential, which is analytic and can be expressed with the Euler Γ function:

$$t = \int_0^{\infty} \exp\left(-\left(\frac{t}{\alpha}\right)^{\beta}\right) dt = \frac{\alpha}{\beta}\Gamma\left(\frac{1}{\beta}\right) \quad (4)$$

In Figure 3 time autocorrelation functions $C(t)$ for the end-to-end vector **L** of the PEO chain in the different systems considered (PEO at water vacuum and PEO at water DMPC interface) are reported. The values are extracted from simulations and fitted using eq 3.

In Table 4, the calculated relaxation times for the different systems have been reported. When the polymer chain is in the presence of an interface, as in the case of systems 2 and 3, relaxation times are calculated separately for the $X-Z$ components and are indicated as τ_X, τ_Y, and τ_Z in Table 4.

In bulk water, the calculated end-to-end relaxation time of the PEO chain is ∼60 ps. In presence of the water/vacuum interface, a value of τ and τ_X and $\tau_Y \sim 60$ ps similar to the bulk water value is obtained. On the contrary, in the direction perpendicular to the water/vacuum interface, a lower value of ∼20 ps is obtained.

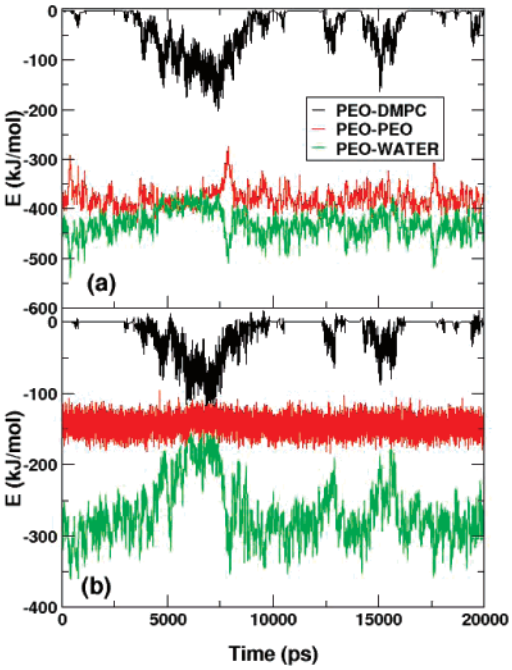

Figure 8. Nonbonded energy contributions: (a) Lennard-Jones and (b) Coulombic terms from simulation of system 2.

PEO at Water/Membrane Interface. *Chain Structure and Dynamics.* The minimum distance and the number of contacts between atoms of PEO and DMPC bilayer during a simulation run of 20 ns are reported in Figure 4a,b, respectively.

A contact is counted if the distance between any atom of PEO and DMPC is within 0.4 nm. From Figure 4b, it is clear that the number of contacts reaches a maximum value of 60 in the interval between 4 and 10 ns. In the following this interval will be denoted as *contact interval*.

In Figure 5 the density distributions of PEO, DMPC, and water, as a function of the Z direction, are shown. The PEO distribution shows a peak in the vicinity of the DMPC interface. The maximum of the PEO density distribution is approximately 1 nm away from the tail of the DMPC bilayer. Considering the radius of gyration (0.7 nm) as an average dimension of the PEO coil, this indicates that the polymer remains mainly close to the interface during the simulation. The end-to-end distance and the radius of gyration of the PEO molecule during the simulation are reported in Figure 6a,b, respectively. As reported in Table 3, the R_g of the PEO averaged over the entire simulation is 0.71 nm. In Table 3, values of R_g and its components averaged over the contact interval have also been reported.

From the plot of Figure 6a, it is apparent that the PEO end-to-end distance shows a maximum value of 3.5 nm in the contact interval. Also in this case the main contribution comes from the elongation along the direction Z perpendicular to the interface. The average value of the Z component of the end-to-end distance in the contact interval is 2 times higher than the X and Y components.

In Figure 7, the XY projected area of the DMPC bilayer versus the simulation time is reported. The time averaged projected area of the DMPC bilayer, in agreement with the experimental value and other theoretical studies,[39] is 0.65 ± 0.01 nm^2/(lipid molecule). In the contact interval, the XY projected area of the DMPC bilayer reaches a minimum; the average value of area/lipid in the contact interval is 0.64 ± 0.01 nm^2/(lipid molecule). The reduction of the XY projected area indicates a tendency of the DMPC bilayer to bend as a consequence of the contacts with PEO.

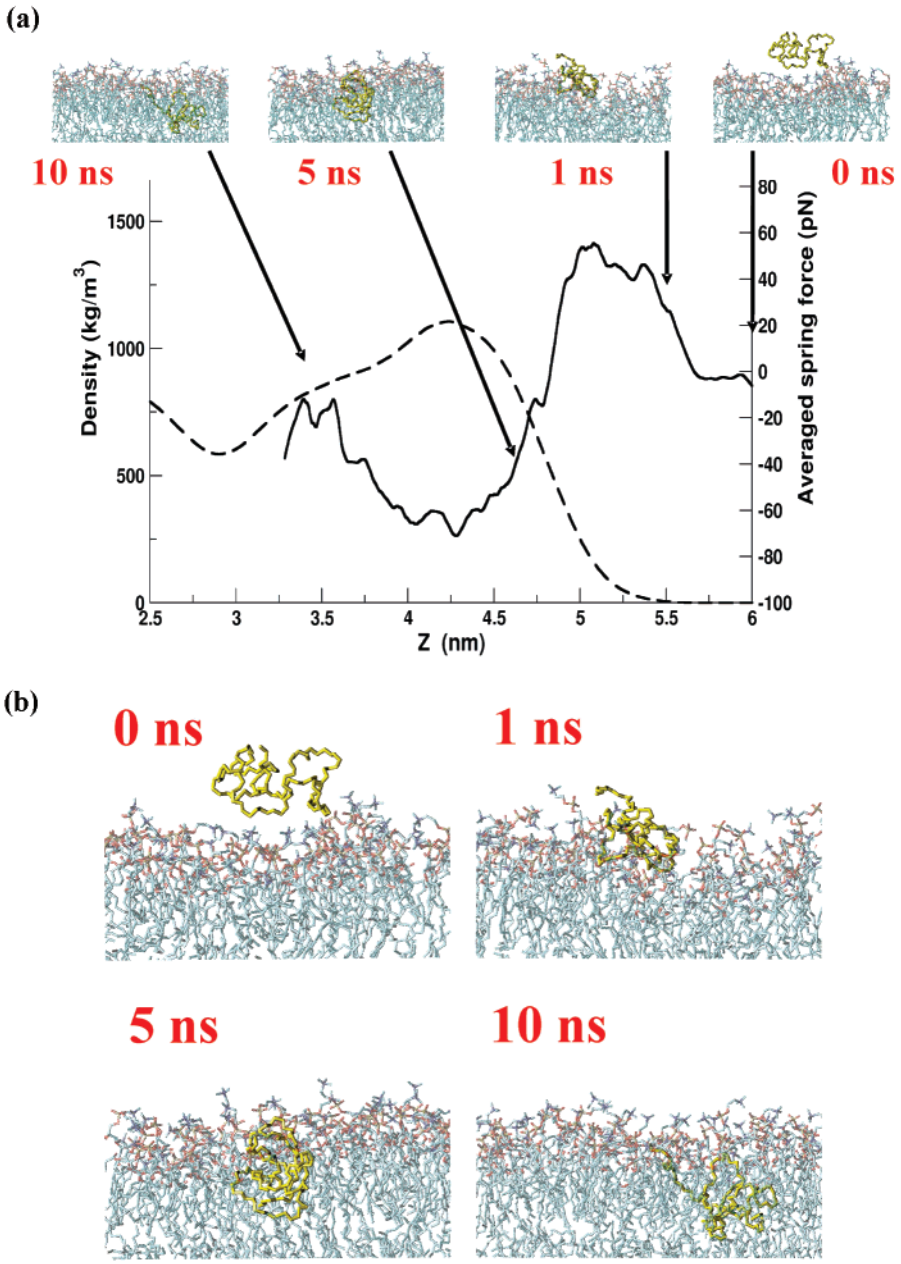

Figure 9. DMPC density profile (dotted line) and the running averaged force from pulling experiments (bold line) versus the *Z* distance of the PEO center of mass. The insets on the top show snapshots of the trajectory along one of the pulling experiments. PEO is represented in yellow.

In Table 4, the calculated end-to-end relaxation times τ, τ_X, τ_Y, and τ_Z of the PEO chain in system 3 are reported. The calculated relaxation time of the PEO chain in the presence of the DMPC bilayer ($\tau \sim 250$ ps) is much higher than the one calculated in bulk water and in the presence of a water/vacuum interface (for both systems 1 and 2, a $\tau \sim 60$ ps has been obtained). In Table 4, values of relaxation times obtained from PEO end-to-end distance autocorrelation functions calculated for system 3 in the contact interval are also reported. In this case, the calculated $\tau \sim 300$ ps is slightly higher than the one obtained from the entire simulation. More interesting is the behavior of the $X-Z$ components of τ**.** The component of τ perpendicular to the interface $\tau_Z \sim 430$ ps is more than four times larger than the ones parallel to the interface τ_X and τ_Y ($\sim$90 ps). In the contact interval, the τ_X and τ_Y become larger ($\sim$140 ps) but still lower than τ_Z.

Finally, it is worth comparing the different behaviors of relaxation time components τ_X, τ_Y, and τ_Z. when the PEO chain is at water/vacuum interface (system 2) and in contact with the DMPC bilayer (system 3). For system 2 with $\tau_Z = 20$ ps, the chain relaxation is faster in the direction perpendicular to the interface. On the contrary, when the chain is in the presence of the lipid bilayer, the relaxation is four times slower in the direction perpendicular to the interface with a $\tau_Z \sim 430$ ps.

Energy Landscape. Figure 8 shows the behavior of different nonbonded energetic contributions (Lennard-Jones and Coulombic energies) during the course of the simulation. In the contact interval, due to the high number of contacts between the polymer chain and the bilayer, both Lennard-Jones and Coulombic contributions of the PEO−DMPC nonbonded energy reach minimum values around −200 and −100 kJ/mol, respectively. The PEO−water Lennard-Jones contribution does not show large variation in the contact interval, while the PEO−water Coulombic contribution increases from approximately −300 to −200 kJ/mol during the contact for the dehydration of the polymer. From Figure 8a, it is clear that the PEO−PEO and PEO−water Lennard-Jones contributions do not show significant variation in the contact interval. A close inspection

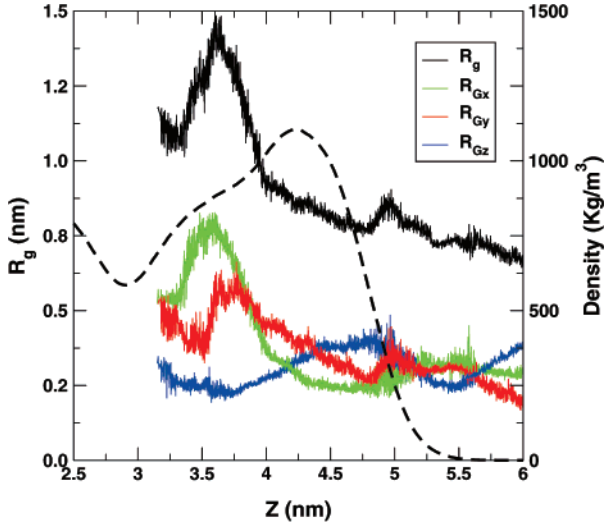

Figure 10. Averaged radius of gyration of the PEO from pulling experiments versus the *Z* distance of the PEO center of mass. The dashed curve indicates the average density profile of the DMPC bilayer.

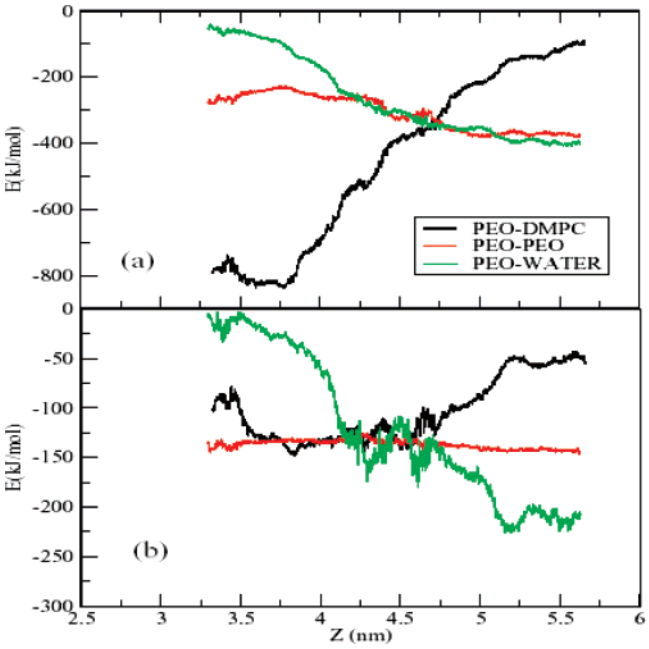

Figure 11. Nonbonded energy contributions: (a) Lennard-Jones and (b) Coulombic terms from the steered molecular dynamics simulation.

of the plot reveals that these two contributions are complementary; small peaks of PEO−PEO Lennard-Jones contribution correspond to almost equal decreases in PEO−water Lennard-Jones.

Steered Molecular Dynamics Simulations. The results of the pulling experiments were analyzed in terms of the spring force, projected *XY* area of the DMPC bilayer, and R_g of PEO versus the *Z* distance of the PEO CoM position. The plots in Figures 9−12 were obtained by making histograms of the instantaneous position along the *Z* coordinates of the PEO CoM. Chain relaxation behavior during the steered MD simulations, due to the applied force on the polymer center of mass, is not reliable and therefore in this section end-to-end time correlation functions have not been evaluated.

In Figure 9, the force on the PEO CoM versus the *Z* position of the PEO CoM is reported. The curve of the force shows that at *Z* greater than 5.7 nm the value of the force is close to zero. For $Z < 5.7$ nm the force on the PEO CoM rises in the positive direction. The increase of the force value is due to the extension

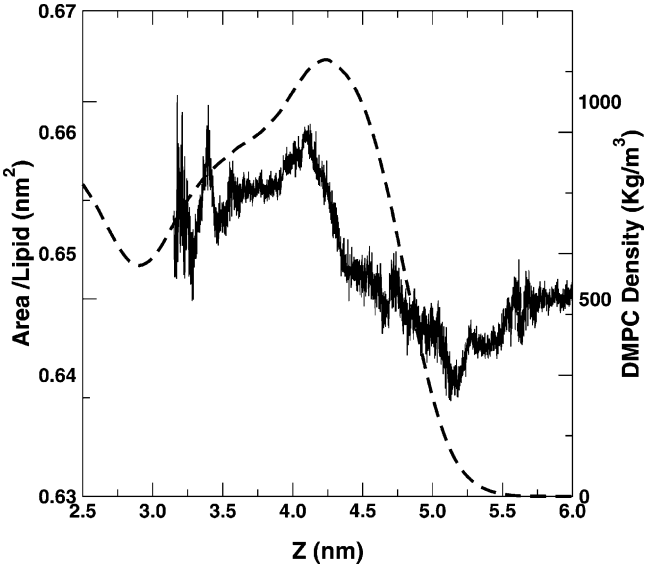

Figure 12. DMPC projected (*XY*) averaged area per lipid from pulling experiments versus the *Z* distance of the PEO center of mass. The dashed curve indicates the average density profile of the DMPC bilayer.

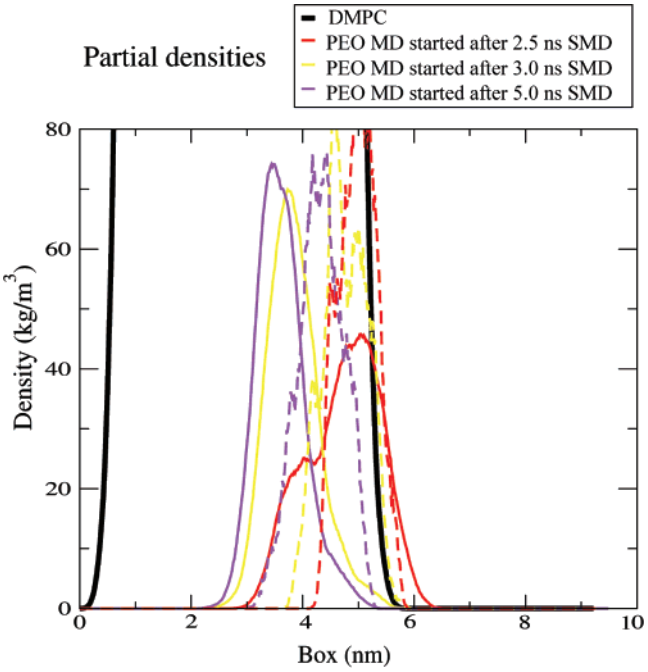

Figure 13. Density distributions along the *Z* axis for PEO and DMPC. PEO density from equilibrium MD simulations started after (a) 2.5 (red curve), (b) 3.0 (yellow curve), and (c) 5 ns (purple curve) of SMD simulation are reported. Continuous lines represent data extracted from an entire 5 ns simulation; broken lines indicate initial densities extracted from the first 500 ps. For the sake of clarity, the density distribution of the DMPC (thick black curve) has been reported from one simulation.

of the spring moving with a constant velocity. The positive increase of the force reaches a maximum value of about 50 pN at $Z = 5.2$ nm that corresponds to a distance of 0.8 nm from the maximum of the density profile of the DMPC bilayer. From Figure 10, it is obvious that the R_g of PEO increases when the PEO CoM comes closer to the membrane. The value of R_g for PEO at $Z > 5.8$ nm is similar to the value obtained from the pure water simulation, indicating the pulling experiments do not affect the conformational equilibrium of the polymer.

As the polymer starts to enter the membrane ($Z < 5.2$ nm), the value of force decreases, implying the presence of an energetic barrier. This fact is also confirmed by the

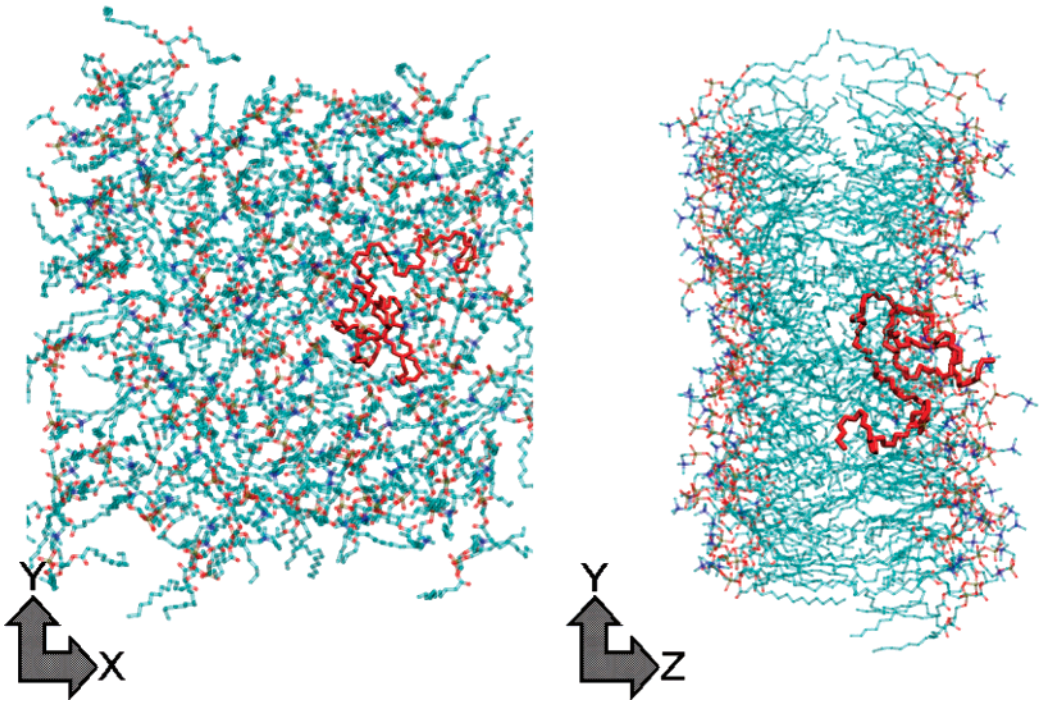

Figure 14. Snapshot of the last configuration (5 ns) from the MD simulation performed starting from the configuration at 2.5 ns of one of the SMD simulations. For the sake of clarity, water molecules are not shown. The PEO chain is colored in red.

PEO−DMPC interaction energy curves in Figure 11. The barrier crossing is followed by a steep decrease in the force value of −70 pN at $Z = 4.2$ nm. The decrease in the force value is reflected by high negative value of PEO−DMPC interaction energy (see Figure 11). By integrating the force versus distance curve (Figure 9), an approximate value of the barrier height equal to 18.6 kJ/mol was calculated. By inspecting Figure 11, it is clear that there is no significant enthalpic barrier to the polymer penetration. This suggests that the calculated barrier is connected to an entropic penalty due to a restriction of polymer conformational freedom inside the bilayer.

At $5.2 < Z < 4.5$ nm the R_g Z component becomes higher than the X and Y components, indicating the extension of the PEO molecule during the crossing of the DMPC monolayer. Once the PEO molecule crosses the barrier, the Z component starts to decrease while the X and the Y components increase.

At $Z > 5.8$ nm, the value of the projected area of the DMPC bilayer (Figure 12) is similar to the value reported for the free simulation. When the PEO molecule encounters the DMPC bilayer and the spring pulls the polymer inside the DMPC bilayer, the projected area of the membrane decreases slightly (0.65 nm^2). The decrease indicates the bending of the DMPC bilayer as the PEO molecule starts to enter the membrane. When the PEO molecule crosses the DMPC bilayer, the area of the membrane increases again and reaches an average value of 0.66 nm^2/(lipid molecule) that is slightly larger than that of the pure membrane.

Once the polymer starts overcoming the monolayer headgroups, the entry of the PEO molecule seems to occur spontaneously. In order to further investigate this point, we have performed three MD simulations starting from three different configurations sampled after 2.5, 3, and 5 ns of one of the SMD simulations. Each simulation was 5 ns long. At the end of the simulation, the density distributions along the Z axis of the polymer, the DMPC, and the water have been calculated after the first 500 ps and for the full trajectory. The results of this analysis are summarized in Figure 13. Broken lines indicate distributions extracted after the first 500 ps, whereas continuous lines are the distribution extracted from the full simulation. For the sake of clarity, the density distribution of the DMPC from only one simulation is reported. The DMPC distributions extracted from other simulations are very similar. From the figure, it is clear that, in all three cases, although the force on the center of mass has been removed, the polymer continues to diffuse into the membrane, depending on the initial position, to different extents. In the case of the starting conformation obtained after 3 and 5 ns of SMD, where the polymer chain is closer to the hydrophobic interior of the membrane, the displacement from the initial position is large. When the polymer center of mass started from a position closer to the membrane surface, the insertion is less pronounced. This is also evidenced by the bimodal distribution of PEO density. These results support a spontaneous entry of the PEO chain after overcoming the monolayer headgroups.

In Figure 14, the polymer chain at the end the MD simulation performed starting from the configuration at 2.5 ns of the SMD simulation has been depicted. From the figure, it is clear that the polymer chain assumes *flower-like* conformations. The flower conformation is characterized by a strongly stretched part and on top of it a crown composed by the remaining chain segments. The configuration of Figure 14 corresponds well with those obtained from Monte Carlo simulations of flexible polymers partially confined into narrow pores.[40,41] Other similarities to these systems have also been found. Free energy increases for insertion of a flexible polymer into a narrow pore calculated by Hermsen et al.,[40,41] using configurational biased Monte Carlo, are comparable with the value we calculated by SMD simulations. In particular, in conditions close to the one experienced by PEO chain crossing the lipid bilayer (pore size smaller than polymer radius of gyration) with an interaction between the polymer and the wall ranging from 0 to 0.8 kT, they found free energy increases of 12 to 5 kT, respectively.

4. Conclusions

In this paper, we have investigated structural and dynamical properties of a PEO/PEG polymer chain at the water/vacuum

and at DMPC bilayer/water interfaces by MD and SMD simulations. A new united atom model of PEO based on OPLS force field has been employed to analyze the PEO/DMPC interactions by performing molecular dynamics simulations of the PEO/DMPC/water system and different steered molecular dynamics pulling experiments of the PEO molecule into the DMPC bilayer. The structural properties of the polymer chain in water and in the presence of the membrane were compared with available experimental data.

The structure and dynamics of a PEO/PEG chain when it is in contact with water/vacuum and DMPC lipid bilayer/water interfaces are different.

At a pure hydrophobic water/vacuum interface the polymer chain is elongated in the *X* and *Y* directions parallel to the interface. In the *Z* direction perpendicular to the interface, the chain is contracted. Furthermore, polymer end-to-end relaxation times of about 60 ps, similar to the bulk water values, have been calculated in the directions *X* and *Y* parallel to the interface**.** In the direction perpendicular to the water/vacuum interface, a lower value of ∼20 ps is obtained.

At DMPC bilayer/water interface the polymer chain is elongated in the direction *Z* perpendicular to the interface, showing a maximum value of end-to-end distance of 3.5 nm in the contact interval.

When the chain is in the presence of the lipid bilayer, the polymer end-to-end relaxation times are higher than those calculated at the water/vacuum interface. Furthermore, the relaxation is four times slower in the direction perpendicular to the interface with a calculated $\tau_Z = 430$ ps.

We also qualitatively analyzed the work necessary to penetrate the bilayer by the PEO chain using SMD simulations. We have found the presence of a barrier for the PEO penetration of the DMPC bilayer. The value of the barrier calculated by integrating the force versus distance curve from the SMD is 18.6 kJ/mol, that is 7 times the value of *kT* at 310 K. This value should be taken "*cum grano salis*" since the nonequilibrium conditions of the SMD simulations could provide an overestimation of energetic barriers. The reported results, in comparison with previous simulations of flexible chains in confined geometry, suggest that the calculated barrier is mainly connected to an entropic penalty due to a restriction of polymer conformational freedom inside the bilayer. Interestingly, once the polymer starts overcoming the monolayer headgroups, the entry of the PEO molecule occurs spontaneously. This strong tendency to interact with the hydrophobic tails inside the lipid bilayer is a consequence of strong LJ interaction energy between the polymer and the tail of the lipids that is responsible for the amphiphilic nature of the polymer.

Acknowledgment. We thank Prof. Florian Müller-Plathe of Technical University of Darmstadt and Tuck Seng Wong and Prof. Martin Zacharias of International University Bremen (IUB) for useful discussions. This study was performed using the computational resources of the CLAMV (Computer Laboratories for Animation, Modeling and Visualization) at IUB, CINECA (Progetti di Supercalcolo convenzione CINECA/ INSTM), and MolNaC (Modeling Lab for Nanostructure and Catalysis, Department of Chemistry, University of Salerno). This work was partially supported by MIUR of Italy (grant PRIN 2002).

References and Notes

(1) Chiellini, E., Migliaresi, C., Sunamoto, J., Eds. *Biomedical Polymers and Polymer Therapeutics;* Kluwer Academic: Dordrecht, The Netherlands, 2001.

(2) Kodera, K.; Matsushima, A.; Hiroto, M.; Nishimura, H.; Ishii, A.; Ueno, T.; Inada, Y. *Prog. Polym. Sci.* **1998**, *23.*

(3) Ringsdorf, H. *Nachr. Chem. Tech. Lab.* **1999**, *8*, 1010.

(4) Lawrence, M. *J. Chem. Soc. Rev.* **1994**, *23*, 417.

(5) Graff, A.; Benito, S.; Verbert, C.; Meier, W. Polymer Nanocontainers. In *Nanobiotechnology. Concepts, Applications and Perspectives*; Miemeyer, C., Mirkin, C., Eds.; Wiley-VCH Verlag: Weinheim, Germany, 2004.

(6) Melik-Nubarov, N.; Pomaz, O.; Dorodnych, T.; Badun, G.; Ksenofontv, A.; Schemchukova, O.; Arzhakov, S. *FEBS Lett. 446*, 194.

(7) Papahadjopoulos, D.; Allen, R.; Gabizon, A.; Mayhew, E.; Matthay, K.; Haung, S.; Lee, K.; Woodle, M.; Lasic, D. D.; Redemann, C.; Martin, F. *Proc. Natl. Acad. Sci. U.S.A.* **1991**, *88*, 11460.

(8) Lee, R. C.; River, L. P.; Pan, F. S.; Ji, L.; Wollmann, R. L. *Proc. Natl. Acad. Sci. U.S.A.* **1992**, *89*, 4524.

(9) Firestone, M.; Wolf, A.; Seifert, S. *Biomacromolecules* **2003**, *4*, 1539.

(10) Firestone, M.; Seifert, S. *Biomacromolecules* **2005**, *4*, 2678.

(11) Szleifer, I. O. V. G.; Thompson, D. H. *Proc. Natl. Acad. Sci. U.S.A.* **1998**, *95*, 1032.

(12) Nielsen, S.; Lopez, C. F.; Srinivas, G.; Klein, M. L. *J. Phys.: Condens. Matter* **2004**, *16*, 481.

(13) Saiz, L.; Klein, M. *Acc. Chem. Res.* **2002**, *35*, 482.

(14) Izrailev, S.; Stepaniants, S.; Isralewitz, B.; Kosztin, D.; H. Lu, F. M.; Wriggers, W.; Schulten, K. Steered Molecular Dynamics. In *Computational Molecular Dynamics: Challenges, Methods, Idea*, Vol. 4; Springer-Verlag: Berlin, Germany, 1998.

(15) Berger, O.; Edholm, O.; Jahnig, J. *Biophys. J.* **1997**, *72*, 2002.

(16) Lindahl, E.; Edholm, O. *Biophys. J.* **2000**, *79*, 426.

(17) Tieleman, D.; Berendsen, H. *J. Chem. Phys.* **1996**, *105*, 4871.

(18) Ryckaert, J. P.; Bellemans, A. *Faraday Discuss. Chem. Soc.* **1978**, *66*, 95.

(19) Jorgensen, W. L.; Tiraldo-Rives, J. *J. Am. Chem. Soc.* **1988**, *110*, 1657.

(20) Jorgensen, W. L. OPLS, Force Field. *Encyclopedia of Computational Chemistry*, Vol. 3; Wiley: New York, 1998; pp 1986−1989.

(21) Nagle, J.; Tristram-Nagle, S. *Biochem. Biophys. Acta* **2000**, *1469*, 1.

(22) Kolafa, J.; Ratner, M. *Mol. Simul.* **1998**, *21*, 1.

(23) Berendsen, H. J. C.; Postma, J. P. M.; van Gunsteren, W. F.; Hermans, J. Interaction Models for Water in Relation to Protein Hydration. In *Intermolecular Forces*; Pullman, B., Ed.; Reidel: Dordrecht, The Netherlands, 1981.

(24) Berendsen, H. J. C.; Postma, J. P. M.; van Gunsteren, W. F.; Di Nola, A.; Haak, J. R. *J. Chem. Phys.* **1984**, *81*, 3684.

(25) Darden, T. A.; York, D. M.; Pedersen, L. *J. Chem. Phys.* **1993**, *98*, 10089.

(26) Ryckaert, J. P.; Ciccotti G.; Berendsen, H. J. C. *J. Comp. Phys.* **1977**, *2*, 327.

(27) Anezo, C.; de Vries, A.; Höltje, H. D.; Tieleman, D.; Marrink, S. J. *J. Phys. Chem. B* **2003**, *107*, 9424.

(28) Miyamoto, S.; Kollman, P. A. *J. Comput. Chem.* **1992**, *13*, 952.

(29) Autenrieth, F.; Tajkhorshid, E.; Schulten, K.; Luthey-Schulten, Z. *J. Phys. Chem. B* **2004**, *108*, 20376.

(30) Gullingsrud, J.; Schulten, K. *Biophys. J.* **2003**, *85*, 2087.

(31) Cheng, F.; Shen, J.; Luo, X.; Jiang, H.; Chen, K. *Biophys. J.* **2002**, *83*, 753.

(32) Shen, L.; Shen, J.; Luo, X.; Cheng, F.; Xu, Y.; Chen, K.; Arnold, E.; Ding, J.; Jiang, H. *Biophys. J.* **2003**, *84*, 3547.

(33) Berendsen, H. J. C.; van der Spoel, D.; van Drunen, R. *Comput. Phys. Commun.* **1995**, *91*, 43.

(34) Lindahl, E.; Hess, B.; van der Spoel, D. *J. Mol. Model.* **2001**, *7*, 306.

(35) Humphrey, W., Dalke, A. and Schulten, K. *J. Mol. Graphics* **1996**, *14*, 33.

(36) Kawaguchi, S.; Imai, G.; Suzuki, J.; Miyahara, A.; Kitano, T.; Ito, K. *Polymer* **1997**, *38*, 2885.

(37) see Rubinstein, M.; Colby, R. H. In *Polymer Physics*; Oxford University Press: Oxford, U.K., 2003

(38) See e.g.: Richter, D.; Dianoux, A. J.; Petry, W.; Teixeira, J. In *Dynamics of Disordered Materials*; Springer-Verlag: Berlin, Germany, 1989.

(39) Anzeco, C.; de. Vries, A. H.; Hoeltje, H.; Tieleman, D. P.; Marrink, S. *J. Phys. Chem. B* **2003**, *107*, 9424.

(40) Hermsen, G. F.; de Geeter, B. A.; van der Vegt, N. F: A.; Wessling, M. *Macromolecules* **2002**, *35*, 5267.

(41) Hermsen, G. F.; Wessling, M.; van der Vegt, N. F. A. *Polymer* **2004**, *45*, 3027.